NATIONAL TRANSPORTATION SAFETY BOARD
Office of Research and Engineering
Washington, D.C. 20594

August 3, 2012

Video Study

NTSB Case Number:
WPR11MA454

A. ACCIDENT

Location:	Reno, Nevada
Date:	September 16, 2011
Time:	16:26 PDT
Aircraft:	North American P-51D, registration: N79111

B. AUTHOR

Dan T. Horak
NTSB
(202) 314-6664
dan.horak@ntsb.gov

C. ACCIDENT SUMMARY

On September 16, 2011, at about 1626 Pacific daylight time, an experimental single seat North America P-51D, N79111, collided with the airport ramp in the spectator box seat area following a loss of control while maneuvering during an unlimited class gold heat race at the National Championship Air Races (NCAR) at Reno Stead Airport (RTS), Reno, Nevada. The airplane was registered to Aero-Trans Corp, Ocala, Florida, and operated by the pilot as Race 177, the Galloping Ghost, under the provisions of 14 *Code of Federal Regulations* (CFR) Part 91. The commercial pilot and 10 people on the ground sustained fatal injuries; more than 60 people were treated for minor to serious injuries. The airplane fragmented upon impact with the ramp. Visual meteorological conditions prevailed and no flight plan had been filed for the local air race flight, which departed RTS about 10 minutes before the accident.

D. DETAILS OF INVESTIGATION

The video of the flight of the accident airplane that was used in this study was recorded by Mr. Jason Schillereff. The video has 720x480 resolution and frame rate of 30 fps. Only every other frame was used in the analysis, resulting in effective frame rate of 15 fps. The total number of analyzed frames was 63. They were spaced by 1/15=0.0667 seconds, resulting in total video analysis time of (63-1)×(1/15)=4.13 seconds. The analyzed time period starts when the airplane was still flying normally along a trajectory that compared well to its trajectories during the first and second laps (the crash occurred during the third lap). This time period includes a roll upset that is the first indication of incipient problems, the time when maximum vertical acceleration occurs, and flight with high angle of climb when the airplane was most likely no longer controlled by the pilot. The airplane crashed about 8 seconds after the end of the analyzed period. The goal of the analysis was to estimate the motion of the airplane and its vertical acceleration (pilot G-force).

Aligning Video Frames with Airplane Locations

The video camera was hand-held and its yaw (azimuth) and pitch (elevation) angles were changing and unknown as it followed the airplane. Aside from the airplane, only clouds were visible in the video. Consequently, terrain features and buildings could not be used to align locations of the airplane with video frames. Therefore, the following reasoning was used to align one specific video frame with one location of the airplane. This video frame was the one where the airplane fuselage was pointed directly into the camera, which could be determined by examining the image of the airplane in the video frames.

Before problems started, the airplane was negotiating a trajectory with a radius of approximately 6450 ft. The radius was estimated based on its GPS locations and comparison with its trajectories during the first and second laps. Therefore, the airplane fuselage heading had to be close to tangential to a trajectory corresponding to a 6450 ft turn radius. Since the camera location was known, the airplane location could be estimated as the location where in a top view a line tangent to the trajectory and passing through the camera location touched the circular trajectory. This provided the alignment between this specific video frame and the corresponding location of the airplane. Aerodynamic analysis indicated that the angle of attack of the airplane was small before problems started and did not affect this method of aligning the video with airplane locations.

The analyzed video segment was only 4.13 seconds long. Therefore, the speed variation during this short period was small. Telemetry data of engine parameters were used to estimate the speed change during the analysis period. The alignment of the one specific video frame and the corresponding airplane location combined with the speed history made it possible to reconstruct the airplane trajectory throughout the entire 4.13 seconds long analysis period, as explained next.

Analysis time 0.0 seconds was set to be slightly before the time when the fuselage pointed directly into the camera. The video frame corresponding to analysis time 0.0 seconds, frame No. 4821, is shown in Fig. 1. It corresponds to telemetry time 16:24:27.00. The last analyzed location, No. 63, corresponds to frame No. 4945. This video frame is shown in Fig. 2.

Figure 1 Video Frame No. 4821 (first analyzed location, time=0.0 s)

Figure 2 Video Frame No. 4945 (last analyzed frame, time=4.13 s)

The roll upset, that is the first indication of incipient problems, becomes clearly visible in frame No. 4889, which is the 35th analyzed frame. It corresponds to time 2.27 seconds in the analyzed interval of 4.13 seconds. This video frame is shown in Fig. 3.

Figure 3 Frame No. 4889 (roll upset becomes visible, time=2.27 s)

Estimating Airplane Motion Based on the Video

The fundamental obstacle to such estimation is the unknown yaw and pitch of the video camera. While the camera location was known and its roll angle was assumed to be zero, its yaw and pitch were not known and were different for each video frame. It was only known that the camera was following the airplane. Therefore, the specific problem was that to estimate the yaw and pitch of the camera, the airplane location was required, and to estimate the airplane location, the camera yaw and pitch were required. A closed-form solution to estimating simultaneously the camera yaw, camera pitch and the airplane location was not possible.

Therefore, the following multi-stage iterative process was developed for estimating the motions of the airplane based on the video.

1. The three Euler angles of the airplane in the camera coordinate system were estimated by aligning a 3D wireframe model of the airplane with its images in the video frames. It was accomplished interactively in a process where the wireframe model was rotated and moved by the user with keystroke commands until alignment was achieved. This had to be done only once for each of the 63 analyzed video frames.
2. The following automatic iterative process was used next.
    a. The airplane was initially assumed to fly along a circular trajectory with a 6450 ft radius and constant altitude, as it approximately did in the first and second lap at the locations recorded in the analyzed video segment.
    b. Camera yaw and pitch were computed to orient the camera at the airplane locations from step (a) on the first pass or step (d) on subsequent passes through the iteration process.

c. The Euler angles in the camera coordinate system were transformed to Euler angles in earth coordinate system, based on the camera yaw and pitch angles from step (b).
d. The airplane trajectory was estimated by integration along its Euler yaw and Euler pitch angle directions computed in step (c) assuming zero angle of attack and zero sideslip angle.
e. The iteration process continued with step (b), unless convergence was achieved as explained in step 3 and the iterative loop was exited.

3. The iteration process was stable mathematically and converged quickly. After five passes through steps (b), (c) and (d), the changes in camera yaw, camera pitch and airplane trajectories were negligible between successive iteration loops.

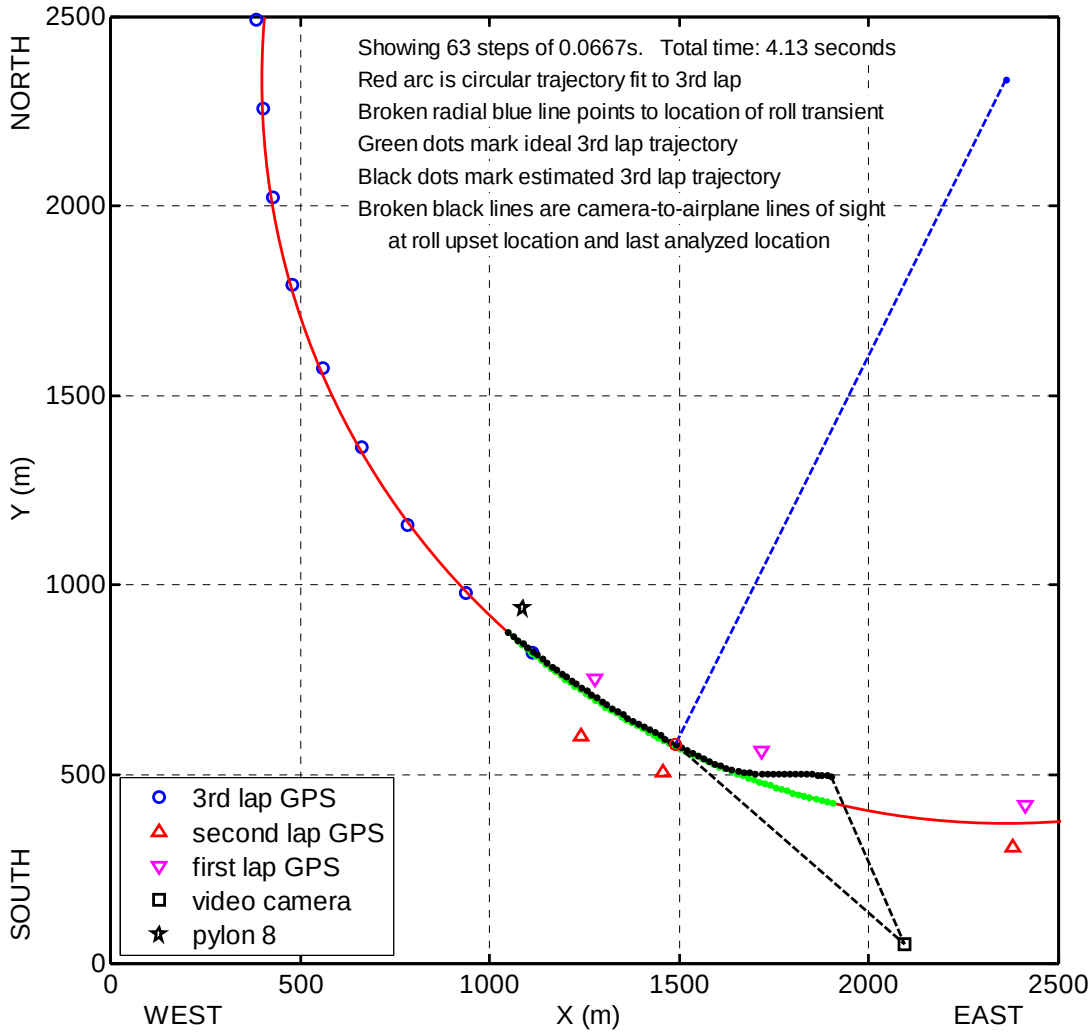

Figure 4 Geometry of the Iterative Airplane Location Estimation Process

Figure 4 shows the geometry of the airplane location estimation problem. Positive X is East and positive Y is North. Point (0,0) is an arbitrary reference point. The top view of the estimated airplane trajectory after the iterative process converged is shown by the black dots, one for each of the analyzed video frames.

Estimating Body-Axis Vertical Acceleration ('Vertical G-Force')

The estimation of the orientation of the airplane in the video was performed using Euler angles. The Euler angles were first estimated in the camera coordinate system and then they were transformed into Earth coordinate system. The effects of G loads on pilots and airplane structures depend on accelerations in airplane body-axis coordinates rather than on their components in the Euler-angle coordinate system. Therefore, after estimating the Euler yaw (ψ), pitch (θ) and roll (ϕ) angles and their rates in the Earth coordinate system, they were used to compute the body-axis angular rates P (roll rate), Q (pitch rate) and R (yaw rate) using Eq. (1).

$$\begin{aligned} P &= d\phi/dt - d\psi/dt \sin\theta \\ Q &= d\theta/dt \cos\phi + d\psi/dt \sin\phi \cos\theta \\ R &= - d\theta/dt \sin\phi + d\psi/dt \cos\phi \cos\theta \end{aligned} \qquad (1)$$

The expression for the body-axis vertical acceleration in units of g is given by

$$a = - (dV/dt \sin\alpha \cos\beta)/g + V \cos\alpha \cos\beta (Q - d\alpha/dt)/g + V \sin\beta (d\beta/dt \sin\alpha - P)/g + \cos\phi \cos\theta \qquad (2)$$

where

P = body-axis roll rate
Q = body-axis pitch rate
R = body-axis yaw rate
a = body-axis vertical acceleration in units of g
V = aircraft speed
α = angle of attack
β = sideslip angle
ϕ = Euler roll angle
θ = Euler pitch angle
ψ = Euler yaw angle
g = acceleration of gravity

Angle of attack α and sideslip angle β cannot be seen in a video. Therefore, they were set to zero in Eq. (2) at this stage of the analysis. The next section in this report details how the effect of these angles was included in the analysis. The resulting equation used for estimating the vertical acceleration with α and β set to zero is Eq. (3).

$$a = VQ/g + \cos\phi \cos\theta \qquad (3)$$

Combining Eq. (1) and Eq. (3) yields the following expression for the body-axis vertical acceleration

$$a = V(d\theta/dt \cos\phi)/g + V(d\psi/dt \sin\phi \cos\theta)/g + \cos\phi \cos\theta \qquad (4)$$

where the first term is the centripetal acceleration due to Euler pitch rate, the second term is the centripetal acceleration due to Euler yaw rate, and the third term is due to gravity. The Euler pitch rate contribution is high when the roll angle is small and $\cos\phi$ is close to one. The Euler yaw rate contribution is high when the roll angle is large and the magnitude of $\sin\phi$ is close to one.

Figure 5 shows the body-axis vertical acceleration during the 4.13 seconds long analysis interval, as estimated with Eq. (4). It also displays its three components shown in Eq. (4). The peak value, at time 3.2 seconds, is 17.3 g. The acceleration increase from the nominal level to the maximum level occurs in about one second.

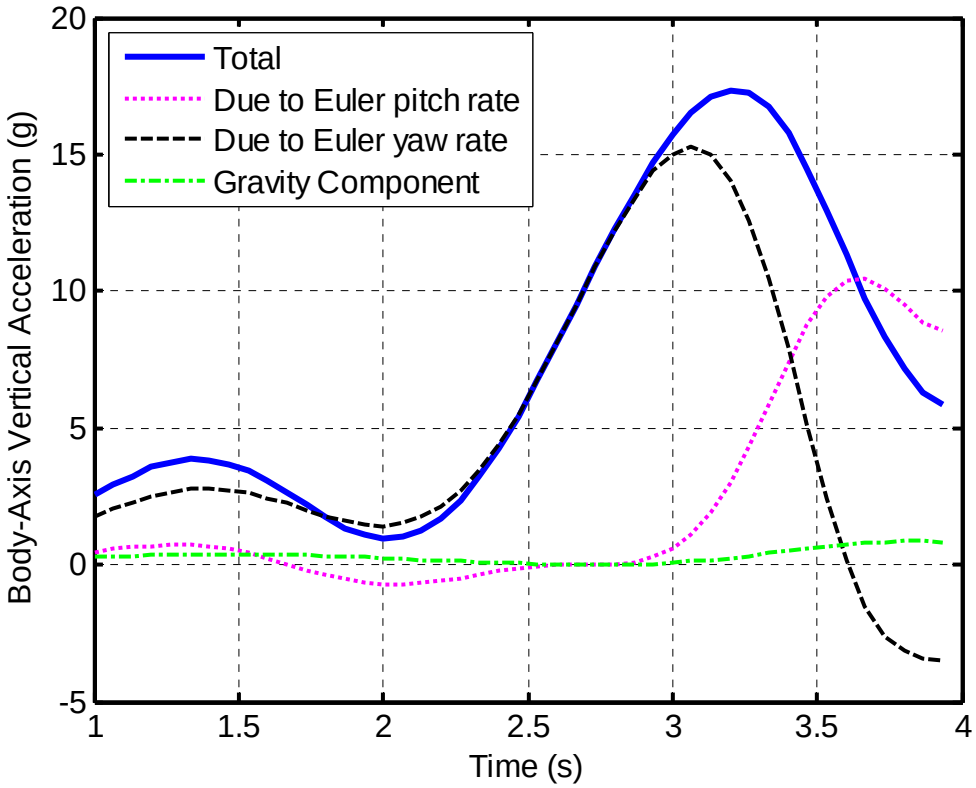

Figure 5 Estimated Body-Axis Vertical Acceleration (G-force)

Figure 5 shows that the main contributor to the total vertical acceleration is the Euler yaw rate component. This component starts increasing about 0.8 seconds before the component due to Euler pitch rate and its magnitude is larger. The increasing magnitude of the Euler yaw angle can be observed in Figure 4 at the location where the

airplane starts turning left and its trajectory starts deviating from the ideal circular trajectory. The magnitude of the roll angle during this turn to the left is high, resulting in the magnitude of $\sin\phi$ in Eq. (4) to be close to 1. Consequently, the Euler yaw rate term contributes significantly to the body-axis vertical acceleration. In most flight situations, the roll angle is small and it is the Euler pitch rate term that contributes significantly to the vertical acceleration while the Euler yaw rate term contribution is small.

During the first 2 seconds, the airplane is flying into the camera, making Euler yaw and Euler pitch angle estimation relatively less accurate because the video frames show mostly the front view of the airplane (see Figure 1). Consequently, it is not possible to determine whether the shape of the acceleration curve in Figure 5 prior to time 2 seconds accurately reflects actual acceleration variations or is due to angle estimation errors. After time 2 seconds, the video frames show more of the side of the airplane, making yaw and pitch angle estimation significantly more accurate. Roll angle could be estimated accurately throughout the analysis period. Both the roll upset and the peak vertical acceleration occurred after time 2 seconds and, therefore, could be estimated accurately.

Estimating the Effect of Angle of Attack and Sideslip Angle on Body-Axis Accelerations

Eq. (3) assumed that the angle of attack and the sideslip angle were zero. However, because of the rapid maneuvering of the airplane visible in Figure 5 and Figure 6, they obviously were not zero.

These angles were estimated using an aerodynamic model of the accident airplane. The modeled airplane was controlled by a simulated pilot model. The simulated pilot actions were computed via feedback laws so as to follow the body-axis angular rates P, Q and R that were estimated in the video analysis.

With non-zero angle of attack and sideslip angle, the trajectory of the airplane estimated via video analysis is slightly different from the trajectory based on them set to zero. The estimated Euler angles are also slightly different. Therefore, an iterative loop was used to derive Euler angles that were in agreement with both the video analysis and the aerodynamic analysis. This was accomplished by using the Euler angle estimates in video analysis in the aerodynamic analysis to derive estimates of the angle of attack and the sideslip angle, and then using these estimates in the video analysis to derive updated Euler angles. This cycle was repeated until the estimates of Euler angles, angle of attack and sideslip angle were no longer changing. Such convergence was achieved in four passes through the iterative loop between video analysis and aerodynamic analysis.

With estimates of angle of attack and sideslip angle available, it became possible to estimate the body-axis vertical acceleration using Eq. (2) rather than using the simplified Eq. (3). Eq. (2) resulted in peak vertical acceleration close to that computed with the simplified equation, Eq. (3).

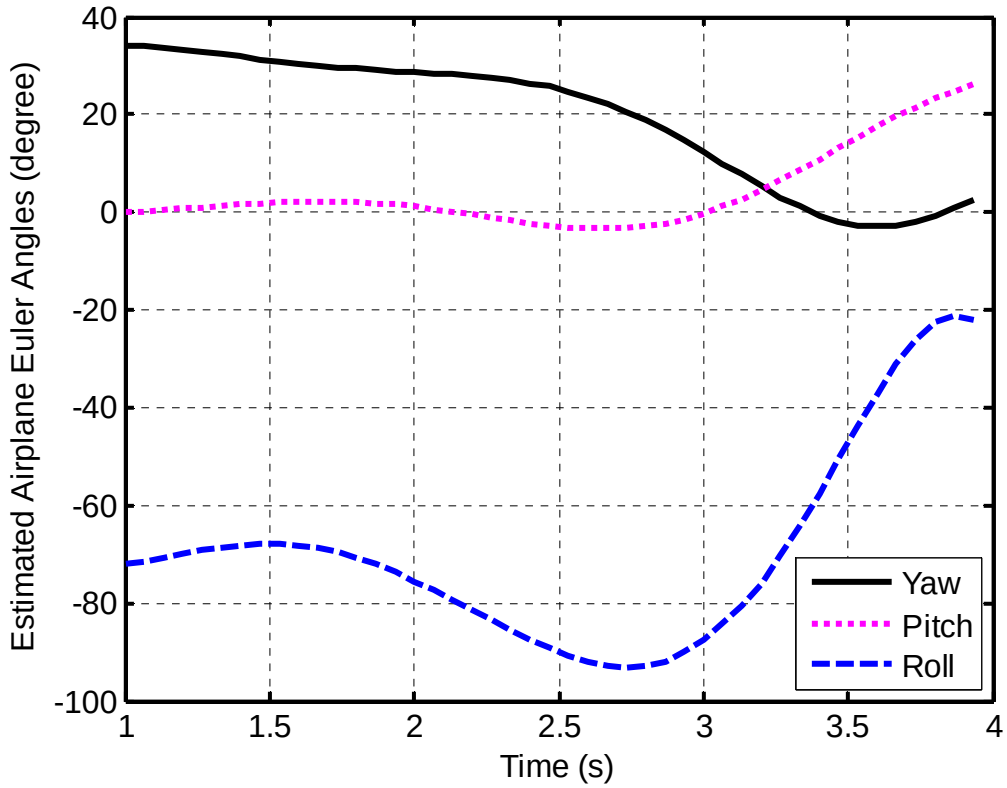

Figure 6 Estimated Airplane Euler Angles

Body-axis lateral acceleration estimate based on assuming that angle of attack and sideslip angle were zero had unrealistically high magnitude before and after the roll upset. When the estimates of angle of attack and sideslip angle derived in the iterative process were taken into account, the magnitude of the estimated body-axis lateral acceleration never exceeded 1 g before the roll upset and was high after the roll upset only when the body-axis vertical acceleration was high. Examination of the lateral acceleration formula revealed that the contribution of $d\beta/dt$ to the lateral acceleration cannot be neglected without generating unrealistically high estimates of the lateral acceleration.

Timing and Magnitude of the Roll Upset

The first indication of incipient problems observed in the video is an increase in the magnitude of the roll angle when its value went from about -70º to about -93º in about one second. Figure 6 shows the estimated roll angle. If the onset of the roll upset is defined as the moment when the roll angle reached -73º, based on the estimated roll angle shown in Figure 6 it happened at time 1.91 seconds. This is earlier than the time estimated just by watching the video. Examination of Figures 5 and 6 shows that the maximum vertical acceleration occurred 0.47 seconds after the roll angle reached its most negative value of -93º (i.e., 93º left wing down).

E. CONCLUSIONS

The first indication of incipient problems was a roll upset during which the airplane reached roll angle of 93º left wing down, its maximum magnitude. Before the upset, the roll angle was about -70º, which is in close agreement with the value estimated using the angle of bank formula.

The body-axis vertical acceleration started increasing when the roll angle magnitude was increasing. The acceleration reached a maximum value of 17.3 g. The maximum acceleration was reached 0.47 seconds after the roll angle magnitude reached its maximum value.

The maximum value of the body-axis vertical acceleration was primarily due to high Euler yaw rate at a time when the magnitude of the roll angle was large.

APPENDIX

The following table lists various variables that were computed in the intermediate and final stages of the analysis described in this study. The variables are defined on page 6. Subscript 'c' refers to camera coordinates and subscript 'e' to earth coordinates.

Time	ψ_c	θ_c	ψ_e	θ_e	ϕ_e	$d\psi_e/dt$	$d\theta_e/dt$	$d\phi_e/dt$	R	Q	P	a
s	*deg*	*deg*	*deg*	*deg*	*deg*	*deg/s*	*deg/s*	*deg/s*	*deg/s*	*deg/s*	*deg/s*	*g*
1.000	-87.0	2.9	34.2	-0.1	-72.1	-4.3	3.6	9.8	2.1	5.2	9.8	2.6
1.067	-86.7	3.2	33.9	0.2	-71.4	-5.0	4.1	11.0	2.3	6.0	11.0	2.9
1.133	-86.3	3.5	33.6	0.5	-70.6	-5.6	4.4	11.3	2.3	6.8	11.4	3.3
1.200	-85.8	3.9	33.2	0.8	-69.9	-6.2	4.7	10.8	2.3	7.4	10.9	3.5
1.267	-85.3	4.2	32.7	1.1	-69.2	-6.6	4.7	9.5	2.1	7.9	9.7	3.8
1.333	-84.7	4.6	32.3	1.4	-68.6	-6.9	4.5	7.5	1.7	8.1	7.7	3.8
1.400	-84.1	5.0	31.8	1.7	-68.2	-7.0	4.1	4.8	1.2	8.0	5.0	3.8
1.467	-83.6	5.3	31.4	1.9	-68.0	-6.9	3.5	1.6	0.6	7.7	1.8	3.7
1.533	-83.0	5.6	30.9	2.1	-68.0	-6.6	2.6	-2.1	-0.1	7.0	-1.8	3.4
1.600	-82.4	5.8	30.5	2.3	-68.3	-6.1	1.5	-6.0	-0.9	6.2	-5.8	3.1
1.667	-81.9	6.0	30.1	2.3	-68.8	-5.6	0.2	-10.1	-1.8	5.3	-9.9	2.6
1.733	-81.3	6.0	29.8	2.3	-69.6	-5.0	-1.2	-14.2	-2.9	4.2	-14.0	2.2
1.800	-80.9	6.0	29.4	2.2	-70.7	-4.4	-2.7	-18.1	-4.0	3.2	-18.0	1.7
1.867	-80.4	5.8	29.2	1.9	-72.0	-3.9	-4.2	-21.8	-5.2	2.4	-21.7	1.3
1.933	-80.0	5.6	28.9	1.6	-73.6	-3.5	-5.6	-25.1	-6.4	1.8	-25.0	1.1
2.000	-79.6	5.3	28.7	1.2	-75.4	-3.4	-6.9	-27.9	-7.5	1.6	-27.8	0.9
2.067	-79.2	4.8	28.5	0.7	-77.3	-3.6	-8.0	-30.0	-8.6	1.7	-29.9	1.0
2.133	-78.8	4.4	28.2	0.1	-79.4	-4.1	-8.8	-31.3	-9.4	2.4	-31.3	1.2
2.200	-78.3	3.8	27.9	-0.5	-81.5	-5.0	-9.2	-31.9	-9.8	3.6	-31.9	1.7
2.267	-77.7	3.3	27.5	-1.1	-83.6	-6.3	-9.2	-31.5	-9.9	5.2	-31.7	2.4
2.333	-77.0	2.7	27.1	-1.7	-85.7	-8.0	-8.8	-30.2	-9.4	7.3	-30.5	3.3
2.400	-76.1	2.2	26.5	-2.3	-87.6	-10.2	-7.9	-27.9	-8.3	9.8	-28.3	4.3
2.467	-75.1	1.8	25.7	-2.7	-89.3	-12.7	-6.5	-24.4	-6.6	12.6	-25.1	5.5
2.533	-73.8	1.4	24.7	-3.1	-90.8	-15.6	-4.5	-19.9	-4.4	15.6	-20.8	6.8
2.600	-72.3	1.2	23.6	-3.3	-92.0	-18.7	-2.2	-14.3	-1.5	18.8	-15.4	8.1
2.667	-70.5	1.1	22.2	-3.4	-92.7	-22.0	0.7	-7.5	1.7	21.9	-8.8	9.4
2.733	-68.4	1.2	20.7	-3.2	-93.0	-25.2	3.9	0.3	5.3	24.9	-1.1	10.7
2.800	-66.0	1.5	18.9	-2.9	-92.6	-28.3	7.4	9.3	8.8	27.9	7.8	12.0
2.867	-63.4	2.1	16.9	-2.2	-91.7	-31.1	11.1	19.2	12.2	30.7	17.9	13.2
2.933	-60.5	2.9	14.7	-1.4	-90.1	-33.4	15.0	29.9	14.9	33.5	29.1	14.4
3.000	-57.4	3.9	12.5	-0.2	-87.7	-35.1	18.8	41.3	17.2	35.9	41.2	15.4
3.067	-54.1	5.2	10.1	1.1	-84.6	-35.9	22.4	53.1	18.8	37.9	53.8	16.3
3.133	-50.7	6.8	7.7	2.7	-80.6	-35.7	25.8	65.0	19.6	39.4	66.7	17.0
3.200	-47.2	8.5	5.3	4.6	-75.9	-34.4	28.7	76.5	19.5	40.2	79.2	17.3
3.267	-43.7	10.5	3.1	6.5	-70.4	-31.8	31.0	87.0	18.7	40.1	90.6	17.3
3.333	-40.4	12.6	1.1	8.7	-64.3	-27.8	32.7	95.9	17.6	38.9	100.1	16.8
3.400	-37.2	14.8	-0.5	10.9	-57.7	-22.6	33.6	102.3	16.6	36.7	106.5	15.9
3.467	-34.4	17.1	-1.8	13.1	-50.8	-16.1	33.8	105.2	16.2	33.5	108.9	14.6
3.533	-31.9	19.5	-2.7	15.4	-43.8	-8.7	33.1	103.8	16.9	29.7	106.1	13.0
3.600	-29.8	21.8	-3.0	17.5	-37.1	-0.5	31.7	97.1	18.7	25.6	97.2	11.3
3.667	-28.2	24.0	-2.7	19.6	-31.0	7.8	29.7	84.1	21.5	21.7	81.5	9.7
3.733	-27.1	26.1	-2.0	21.5	-26.0	15.6	27.3	64.3	25.0	18.2	58.6	8.3
3.800	-26.3	28.2	-0.7	23.2	-22.6	22.0	25.0	37.7	28.2	15.4	29.1	7.1
3.867	-25.8	30.1	0.9	24.8	-21.1	25.9	23.2	5.3	30.2	13.2	-5.6	6.2
3.933	-25.4	31.9	2.7	26.3	-21.9	25.8	22.5	-30.8	29.8	12.2	-42.3	5.8